Deep 3D convolutional neural network applied to CT segmented image for rock properties prediction

Leandro Passos de Figueiredo, Fernando Bordignon and Rodrigo Exterkoetter, LTrace Geophysical Solutions; Bruno Barbosa Rodrigues and Maury Duarte, Petrobras*

SUMMARY

Digital rock physics is a promising method for rock properties prediction based on imaging and computer simulation of digital rock models. In this work we propose a deep convolutional neural network (CNN) to estimate the distribution of porosity and P-wave velocity from a segmented CT 3D image of a rock sample. The proposed CNN applies 3D convolutional filters to extract and identify the most important features of the grain and pore structures of the rock. The training dataset is generated based on idealized rock models of random sphere packing, which allows the analytical computation of the target properties. We apply the trained CNN to two real segmented CT images of Berea sandstone to validate the proposed approach. The results show that the approach is computationally efficient to estimate the rock properties and it can be used for testing and validating of different segmentation methods.

INTRODUCTION

Digital rock physics is an innovative approach based on imaging and digitalizing the rocks under study for simulating and computing their properties such as total and effective porosity, grain size, permeability and elastic moduli (Andrä et al., 2013; Sudakov et al., 2019). The imaging of a rock sample is performed trough several projections of the rock sample that allows the visualization of the 3D micro structure of the rock. With the segmentation process, we obtain a digital rock model where the mineral phases and the pore space are characterized. The 3D representation of the rock is later used to simulate physical processes with the aim to predict several rock properties (Chauhan et al., 2016; Blunt et al., 2013).

With the improvements in acquisition and processing seismic data in the last decades, the understanding of the relations between the rock properties have became crucial (Avseth et al., 2005). The rock-physics models provide the theoretical basis to transform one rock attribute to another. We can find several applications of different rock-physics models for seismic interpretation and reservoir characterization (Bachrach, 2006; Grana and Della Rossa, 2010; Wilkins and Pambayuning, 2016; de Figueiredo et al., 2018). In general, the rock-physics model depends on the basic components and characteristics of the rocks, such as mineral, fluid, grain shape and cementation (Mavko et al., 2009; Dvorkin et al., 2014). Since the models are supported by theoretical relations and basic knowledge about the rocks, the models allow us to extend the understating of the subsurface beyond the original observations (Dvorkin et al., 2014).

This work proposes a deep learning-based approach for determining the porosity and the P-velocity from a segmented micro CT rock sample. Synthetic idealized rock models based on random sphere packing are generated to train a 3D convolutional neural network (CNN) (Ji et al., 2013). The training is performed by providing 3D images of the idealized rock for the CNN with the respective output properties, which are calculated according to an analytical rock-physics model. In the methodology section we first introduce the basic theory of the used rock-physics model, and then we discuss how we generate the entire dataset. The application section includes the discussion of the proposed approach applied to two segmented CT images of the Berea sandstone.

METHODOLOGY

Sedimentary rocks are often idealized as a sphere packing with a given cementation and compaction level (Mavko et al., 2009; Dvorkin et al., 2014). The main advantage of this representation is the analytical treatment of the mechanical interactions of the grains under stress, which allows obtaining the analytical expression of several properties of the rock. Based on these theoretical results of rock-physics models, we generate the training dataset of the CNN to predict the rock properties by applying the CNN to the real micro CT of sedimentary rocks.

Rock-physics

The Hertz-Mindlin model allows us to calculate the effective bulk and shear modulus (K_{HM} and μ_{HM}, respectively) of a dry, random and identical sphere packing for a given hydrostatic confining pressure P, critical porosity ϕ, grain shear modulus μ and the grain Poisson ratio ν. The porosity of a packing with identical spheres depends only on how the grains are organized. To find the effective moduli at different porosity values, caused by cementation, the Hashin-Shtrikman lower and upper bounds can be applied:

$$K_{eff} = \left[\frac{\phi/\phi_0}{K_{HM} + \frac{4}{3}\mu_i} + \frac{1-\phi/\phi_0}{K + \frac{4}{3}\mu_i} \right]^{-1} - \frac{4}{3}\mu_i \qquad (1)$$

$$\mu_{eff} = \left[\frac{\phi/\phi_0}{\mu_{HM} + \frac{\mu_i}{6}\left(\frac{9K_i+8\mu_i}{K_i+2\mu_i}\right)} + \frac{1-\phi/\phi_0}{\mu_i + \frac{\mu_i}{6}\left(\frac{9K_i+8\mu_i}{K_i+2\mu_i}\right)} \right]^{-1} - \frac{\mu_i}{6}\left(\frac{9K_i+8\mu_i}{K_i+2\mu_i}\right) \qquad (2)$$

where $K_i = K_{HM}$ and $\mu_i = \mu_{HM}$ for the Hashin-Shtrikman lower bound (soft-sand model), or $K_i = K$ and $\mu_i = \mu$ for the upper bound (stiff-sand model), and K and μ are the moduli of the grains. The physical interpretation of the soft-sand model is when the cement is deposited away from the grain contacts, whereas of the stiff-sand model is when the cement is in contact with the grains (Mavko et al., 2009; Dvorkin et al., 2014).

10.1190/segam2019-3216835.1

Since we have the elastic moduli of the rock, we can calculate the seismic P-wave velocity in terms of the petrophysical and structural variables of the rock:

$$V_p = \sqrt{\frac{K_{eff} + \frac{4}{3}\mu_{eff}}{\rho}}, \quad (3)$$

where ρ is the rock density

$$\rho = (1-\phi)\rho_m \quad (4)$$

and ρ_m is the density of the mineral phase.

Synthetic data generation

The generation of the training dataset starts with a random sphere packing. Using the algorithm from Baranau and Tallarek (2014) we generate a $1000 \times 1000 \times 1000$ pack with approximately 10 thousand identical spheres with radii of 50. The pack has an experimental porosity of 0.355, which it is in accordance to the expected theoretical porosity of 0.36. Figure 1 shows a slice of the 3D pack of spheres.

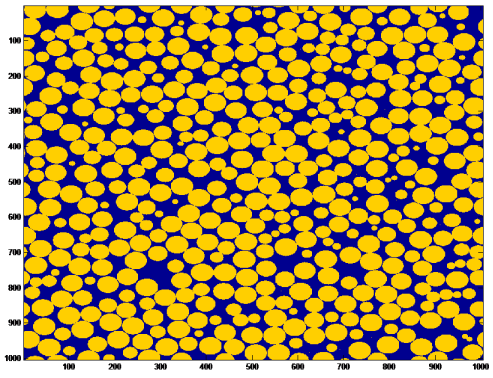

Figure 1: 2D slice of the 3D pack of spheres.

By assigning a voxel size of $0.001mm^3$ to the packing image all the spheres have a fixed diameter of $0.05mm$. To cover a range of possible grain size, the 3D image of the random packing is scaled g times while maintaining the voxel size in millimeters. Ideally, the minimum and maximum grain sizes must include the range reported at the literature for the rock under study. With this step, we obtain g 3D images of the sphere packing for difference sphere sizes and same porosity of 0.355.

To obtain different porosity values for the sphere packing images generated in the first step, we propose to simulate a different cementation levels among the spheres. The cementations are simulated based on the physical interpretation of the soft and stiff sand model. We generate p levels of porosity to cover the possible range of porosity values, typically from 0 to the critical porosity (0.36 for random sphere packing).

For the soft sand model, where the cement is interpreted to be away from the grain contacts, it is simulated by randomly flipping the necessary number of pore voxels, away at least 1 voxel from the grains, to reach the desired porosity level. Similarly, for the stiff-sand model, the cementation is simulated by using Truncated Gaussian Simulation (Armstrong et al., 2011) with an unconstrained geostatistical simulation method such as FFT-MA (Ravalec et al., 2000) or SGS (Deutsch and Journel, 1992). A spherical variogram of range equal to half of the grain size and variance equal to one is used. The threshold applied for the truncation of the Gaussian simulation is defined as

$$l = c^{-1}(1-\phi_i/\phi_p), \quad (5)$$

where $c^{-1}(.)$ is the inverse normal cumulative function, ϕ_i is the desired porosity level and ϕ_p is the porosity of the sphere pack. The voxel-wise OR operation is applied to the binarized simulation and the sphere pack. Figure 2 shows examples of 2D slices from the 3D images for 3 levels of porosity and grain sizes.

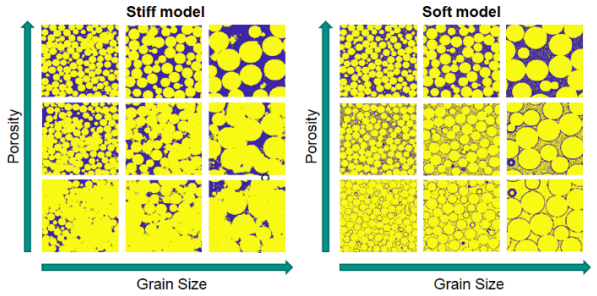

Figure 2: Slices from 3D examples of the two types of cementation and three levels of porosity and grain sizes.

The two described cementation simulations are repeated p times with different levels of porosity for each of the g scaled models obtained in the last step, resulting in $2pg$ synthetic binary segmented images. For each image, we have a known grain size, porosity label, a flag indicating the cementation type (soft or stiff) and P-wave velocity, which is calculated by Equation 3 according to the discussed rock-physics model.

The last step for the training is the subsampling of small 3D windows with dimension of w^3 from the obtained 3D models of the cemented random sphere packing. A number s of samples per case is chosen (≈ 500) and the total number of training samples is $2pgs$. The subsampling will result in a smaller 3D window that have 3 labels: the porosity, which changes locally for each window; the model type (stiff or soft); and the P-wave Velocity. The porosity label is recalculated using the respective subsample and P-wave velocity is calculated with the corresponding rock-physics model using the local porosity and a minerals parameterization that should be in accordance to the mineral in the rock sample.

Usually, the dimension of the experimental micro-CT images are higher than the used window dimension (typically $w < 128$ due to computational limits). Then, the CNN is applied to a moving window of the original micro-CT image with dimension w^3. As a result of the CNN, we have a predicted porosity, P-wave velocity and soft/stiff label for each subsample of the original image. The multiple predictions for the same micro-CT image under study can be interpreted as the property dis-

10.1190/segam2019-3216835.1

tribution of the rock sample, as long as the window has a minimum size that is representative of the rock.

3D Convolutional Neural Network

A 3D CNN can extract spatial features from 3D images by performing 3D convolutions. Applications involve spatial pattern recognition and identification, feature learning and non linear regression fitting (Ji et al., 2013). In this work, the 3D CNN was used for learning the porosity, cementation type and P-velocity from stiff and soft segmented models. Table 1 shows the layers of the network used, its size and the total number of parameters. All layers have Rectified Linear Unit (ReLU) activations (Nair and Hinton, 2010) except for the last one that uses Hyperbolic Tangent (tanh).

#	Type	Stride	Filters	Parameters
1	Convolutional 3D	2x2x2	8	224
2	Convolutional 3D	No	16	3,472
3	Convolutional 3D	2x2x2	32	13,856
4	Convolutional 3D	No	64	55,360
5	Convolutional 3D	2x2x2	64	110,656
6	Convolutional 3D	No	128	221,312
7	Convolutional 3D	No	128	442,496
8	Convolutional 3D	No	3	387
		Total:	443	847,763

Table 1: 3D CNN layers.

In many cases, popular layers like pooling layers are used to increase deep neural networks performance (Ji et al., 2013). Pooling layers decreases the size of the feature maps by pooling the maximum activation of the previous layers, improving gain in invariance to certain input transformations but compromising on precision (Springenberg et al., 2014). In this work, due to the need of precise information about rock properties present in micro-CT, the 3D CNN model was built without these type of layers.

The input layer size can be changed as needed depending on the study. A recommendation is to choose a window size that fits at least a few average-sized grains, in order to CNN properly infer the outputs not only by the segmentation values itself, but by using also the shape of the grains and pores. In this case, from visual inspections and tests, we've chosen to use $w = 64$.

EXPERIMENTS

The methodology is applied to two different segmentations of Berea sandstone CT image by Dong and Blunt (2009) and Andrä et al. (2013), which for simplicity we call them by Segmentation 1 and Segmentation 2, respectively. Figure 3 shows both segmentation side by side with the same scale for comparison.

For the training dataset we consider $g = 5$ scale factors and $p = 5$ cementation levels, varying the expected porosity from 0.05 to 0.30. For each of the $2pg$ images, we randomly select

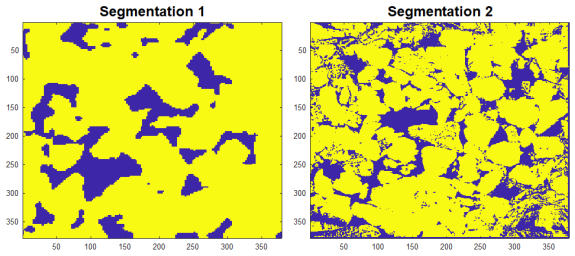

Figure 3: Segmented CT images used for validation of the proposed deep learning approach for rock properties prediction.

600 subsamples with dimension of $64 \times 64 \times 64$ resulting in a total of 30,000 3D training images with the respectively results of porosity, P-wave velocity and stiff/soft cementation label. Based on previous studies on the Berea sandstone (Churcher et al., 1991; Dong and Blunt, 2009; Andrä et al., 2013; Huang et al., 2017), for the calculation of P-wave velocity, we apply the rock physics models by using the mineral parameters of quartz, shown in table 2 below.

Parameter	Value
Bulk modulus	37 GPa
Shear modulus	40 GPa
Density	2.65 g/cm^3
Coordination #	9
Pressure	20 MPa
Critical porosity	0.36

Table 2: Rock physics parameters of the mineral phase (Quartz).

After training the CNN we applied it to 5,000 subsamples of the real segmented micro-CT images. The results for porosity and P-wave velocity are in Figure 4 and 5, respectively. Both figures show the histogram of the properties predicted for all the subsamples, the histogram obtained for segmentation 1 is in yellow and for segmentation 2 is in blue. The same output results are shown in the cross-plot of porosity and P-wave velocity in Figure 6, with the respective colors for each segmentation. We can observe that the CNN predicts P-wave velocities closer to the stiff sand model for both segmentations.

Despite not having the actual velocity of low frequency (2-800Hz) P-waves for each rock sample of the micro-CT images, we compare the results to the reference value obtained by Huang et al. (2017). The measured P-wave velocity varies in terms of the wave frequency and pressure. Assuming a pressure of 20 MPa, the velocity is approximately 3600 m/s and it is approximately constant up to 100Hz. The porosity reference value of Berea sandstone is around 20% but it also varies from one sample to another (Churcher et al., 1991; Dong and Blunt, 2009; Andrä et al., 2013; Huang et al., 2017). In table 3 we compare the reference values to the average values obtained by the CNN applied in both segmented images. We observe that the predicted values are in accordance to the reference properties but for the segmentation 1 the CNN presents

10.1190/segam2019-3216835.1

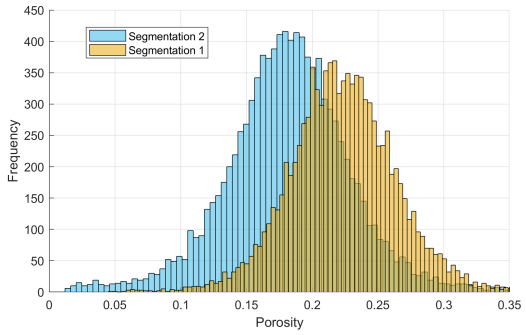

Figure 4: Histogram of porosity values obtained by the CNN for the two segmented images. Result for segmentation 1 is in yellow and for segmentation 2 is in blue.

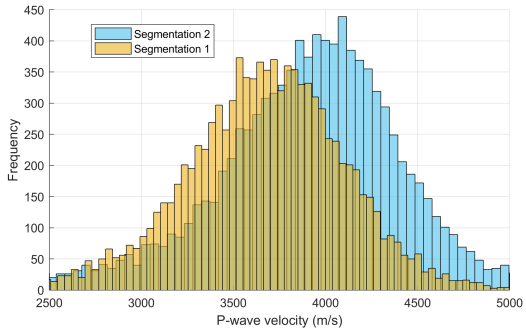

Figure 5: Histogram of P-wave velocities obtained by the CNN for the two segmented images. Result for segmentation 1 is in yellow and for segmentation 2 is in blue.

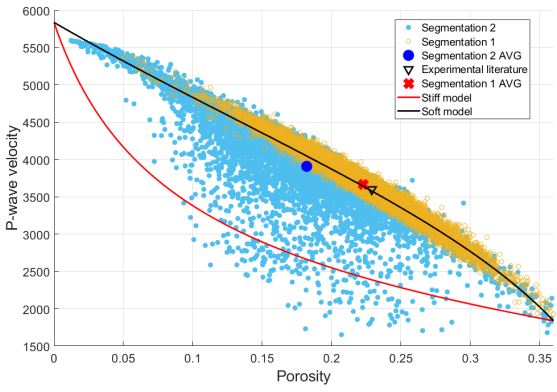

Figure 6: Cross-plot of porosity versus P-wave velocity: CNN output for segmentation 1 in yellow with average value in red dot; for segmentation 2 in blue with average value in dark blue dot; black triangle shows the reference values of porosity and P-wave velocity; solid curves are the theoretical rock-physics models, stiff sand model in black and soft sand model in blue.

a better prediction of P-wave velocity and porosity.

Property	Reference	Seg. 1	Seg. 2
Porosity (%)	19–23	22.3	18.21
P-wave velocity (m/s)	3600–3800	3664	3908

Table 3: Comparison of the predicted results to the reference properties of the Berea sandstone.

CONCLUSION

We propose a deep learning approach for rock properties prediction based on CT segmented images. The training dataset of the 3D CNN is generated based on idealized rock models of random sphere packing. The advantage of idealized rock models is the analytical treatment of the rock properties, which is used as the final expected result of the training dataset. We apply the CNN to two segmented images of Berea sandstone. The predicted porosity and P-wave velocity is in accordance to the reference values in the literature. The obtained results indicate that the approach is sensitive to the segmentation method and it can be a practical tool for testing and validating different segmentation methods, by comparing the predictions to the reference values of the rock-sample. Further studies can be done with the objective to analyse carbonate rock samples by using the physical interpretation of theoretical inclusion rock-physics models.

ACKNOWLEDGEMENTS

The authors would like to acknowledge PETROBRAS for the availability and technical support during the development of this work.

10.1190/segam2019-3216835.1

REFERENCES

Andra, H., N. Combaret, J. Dvorkin, E. Glatt, J. Han, M. Kabel, Y. Keehm, F. Krzikalla, M. Lee, C. Madonna, M. Marsh, T. Mukerji, E. H. Saenger, R. Sain, N. Saxena, S. Ricker, A. Weigmann, and X. Zhan, 2013, Digital rock physics benchmarks Part — I: Imaging and segmentation: Computers and Geosciences, **50**, 25–32, doi: 10.1016/j.cageo.2012.09.005.

Armstrong, M., A. Galli, H. Beucher, G. Loc'h, D. Renard, B. Doligez, R. Eschard, and F. Geffroy, 2011, Plurigaussian simulations in geosciences: Springer Science and Business Media.

Avseth, P., T. Mukerji, and G. Mavko, 2005, Quantitative interpretation: Cambridge University Press.

Bachrach, R., 2006, Joint estimation of porosity and saturation using stochastic rock-physics modeling: Geophysics, **71**, no. 5, O53–O63, doi: 10.1190/1.2235991.

Baranau, V., and U. Tallarek, 2014, Random-close packing limits for monodisperse and polydisperse hard spheres: Soft Matter, **10**, 3826–3841, doi: 10.1039/c3sm52959b.

Blunt, M. J., B. Bijeljic, H. Dong, O. Gharbi, S. Iglauer, P. Mostaghimi, A. Paluszny, and C. Pentland, 2013, Pore-scale imaging and modelling: Advances in Water Resources, **51**, 197–216, doi: 10.1016/j.advwatres.2012.03.003.

Chauhan, S., W. Ruhaak, F. Khan, F. Enzmann, P. Mielke, M. Kersten, and I. Sass, 2016, Processing of rock core microtomography images: Using seven different machine learning algorithms: Computers and Geosciences, **86**, 120–128, doi: 10.1016/j.cageo.2015.10.013.

Churcher, P., P. French, J. C. Shaw, and Schramm, 1991, Rock properties of Berea sandstone, baker dolomite, and Indiana limestone: A paper prepared for presentation at the SPE International Symposium on Oilfield Chemistry, 431–446.

de Figueiredo, L. P., D. Grana, F. L. Bordignon, M. Santos, M. Roisenberg, and B. B. Rodrigues, 2018, Joint Bayesian based inversion on rock-physics prior modeling for the estimation of spatially correlated reservoir properties: Geophysics, **83**, no. 5, M49–M61, doi: 10.1190/geo2017-0463.1.

Deutsch, C., and A. G. Journel, 1992, Gslib: Geostatistical software library and users guide: Oxford University Press. Centre de Morphologie Mathematique Fontainebleau: Les cahiers du Centre de Morphologie Mathematique de Fontainebleau.

Dong, H., and M. J. Blunt, 2009, Pore-network extraction from micro-computerized-tomography images: Physical Review E, **80**, no. 3, 036307, doi: 10.1103/PhysRevE.80.036307.

Dvorkin, J., M. Gutierrez, and D. Grana, 2014, Reflections of rock properties: Cambridge University Press.

Grana, D., and E. Della Rossa, 2010, Probabilistic petrophysical-properties estimation integrating statistical rock physics with: Geophysics, **75**, no. 3, O21–O37, doi: 10.1190/1.3386676.

Huang, Q., D.-H. Han, H. Yuan, Q. Wei, and M. Sun, 2017, Velocity dispersion and wave attenuation of Berea sandstone at different saturations and pressures in frequency band: 87th Annual International Meeting, SEG, Expanded Abstracts, 3574–3578, doi: 10.1190/segam2017-17787584.1.

Ji, S., W. Xu, M. Yang, and K. Yu, 2013, 3D convolutional neural networks for human action recognition: IEEE Transactions on Pattern Analysis and Machine Intelligence, **35**, 221–231, doi: 10.1109/TPAMI.2012.59.

Mavko, G., T. Mukerji, and J. Dvorkin, 2009, The rock physics handbook: Tools for analysis of porous media: Cambridge University Press.

Nair, V., and G. E. Hinton, 2010, Rectified linear units improve restricted Boltzmann machines: Proceedings of the 27th International Conference on Machine Learning, 807–814.

Ravalec, M. L., B. Noetinger, and L. Y. Hu, 2000, The FFT moving average (FFT-MA) generator: An efficient numerical method for generating and conditioning Gaussian simulations: Mathematical Geology, **32**, 701–723, doi: 10.1023/A:1007542406333.

Springenberg, J. T., A. Dosovitskiy, T. Brox, and M. Riedmiller, 2014, Striving for simplicity: The all convolutional net: arXiv preprint arXiv:1412.6806.

Sudakov, O., E. Burnaev, and D. Koroteev, 2019, Driving digital rock towards machine learning: Predicting permeability with gradient boosting and deep neural networks: Computers and Geosciences, **127**, 91–98, doi: 10.1016/j.cageo.2019.02.002.

Wilkins, M., and S. Pambayuning, 2016, Rock physics applications for interpretation in the gulf of Thailand: Presented at the International Petroleum Technology Conference.